Source and formation characteristics of water-soluble organic carbon in the anthropogenic-influenced Yellow River…

Article *in* Atmospheric Environment · November 2016

DOI: 10.1016/j.atmosenv.2016.08.078

7 authors, including:

Chongguo Tian
Chinese Academy of Sciences
71 PUBLICATIONS **484** CITATIONS
SEE PROFILE

Yingjun Chen
Tongji University
78 PUBLICATIONS **1,666** CITATIONS
SEE PROFILE

Jun Li
Chinese Academy of Sciences
217 PUBLICATIONS **4,034** CITATIONS
SEE PROFILE

Gan Zhang
Chinese Academy of Sciences
370 PUBLICATIONS **10,310** CITATIONS
SEE PROFILE

Atmospheric Environment 144 (2016) 124–132

Contents lists available at ScienceDirect

Atmospheric Environment

journal homepage: www.elsevier.com/locate/atmosenv

Source and formation characteristics of water-soluble organic carbon in the anthropogenic-influenced Yellow River Delta, North China

Zheng Zong [a, d], Xiaoping Wang [b], Chongguo Tian [a, *], Yingjun Chen [c, **], Guangxuan Han [a], Jun Li [b], Gan Zhang [b]

[a] Key Laboratory of Coastal Environmental Processes and Ecological Remediation, Yantai Institute of Coastal Zone Research, Chinese Academy of Sciences, Yantai, 264003, China
[b] State Key Laboratory of Organic Geochemistry, Guangzhou Institute of Geochemistry, Chinese Academy of Sciences, Guangzhou, 510640, China
[c] Key Laboratory of Cities' Mitigation and Adaptation to Climate Change in Shanghai (CMA), College of Environmental Science and Engineering, Tongji University, Shanghai, 200092, China
[d] University of Chinese Academy of Sciences, Beijing, 100049, China

HIGHLIGHTS

- High intensity measurement of WSOC in $PM_{2.5}$ was conducted at Yellow River Delta.
- WSOC concentration in day time was obviously higher than night time.
- WSOC was mostly secondary formation product and was enhanced at high level of acidity.
- Biogenic and biomass burning (B&B) was the major source of WSOC.
- Fossil fuel contribution, mainly vehicle emission, could not be ignored.

ARTICLE INFO

Article history:
Received 2 August 2016
Received in revised form
26 August 2016
Accepted 30 August 2016
Available online 31 August 2016

Keywords:
WSOC
Aerosol acidity
Source apportionment
^{14}C measurement

ABSTRACT

High intensity measurement of water-soluble organic carbon (WSOC) in $PM_{2.5}$ was conducted at Yellow River Delta (YRD), North China, from 29 May to 1 July 2013. On average, concentration of WSOC was 3.09 ± 2.45 μg m^{-3} with a relative high WSOC/OC mass ratio (56.39%), implying organic aerosol in YRD was aged. WSOC concentration in day time was obviously higher than night time, which was mainly attributed to the decrease of source emission. While secondary formation of WSOC was strengthen in night time under stable atmospheric condition. The significant relationship between WSOC and SOC indicated WSOC was mostly secondary formation product. Furthermore, WSOC formation was enhanced at high level of acidity, providing direct evidence for the great impact of aerosol acidity on WSOC formation. WSOC correlated well with nss-K^+, nss-SO_4^{2-}, NO_3^-, Zn and Cu, suggesting a major part of observed WSOC and/or its precursors was of biomass burning and fossil fuel combustion origin. Moreover, vehicle emission may make great proportion in the fossil fuel combustion. Conditional probability function (CPF) analysis showed significant contribution of WSOC occurred when wind came from southerly (135–195°) and northwesterly (285, 345°) directions. In order to further confirm the source of WSOC, two merged samples representing the two directions were selected for radiocarbon (^{14}C) measurement. ^{14}C results demonstrated the average value of f_c(WSOC) was 0.57 ± 0.01, implying biogenic and biomass burning (B&B) was the major source of WSOC. However, fossil fuel contribution could not be ignored in North China in summer.

1. Introduction

Recent years, increasing attention has been focused to water-soluble organic carbon (WSOC), which constitutes a substantial fraction of carbonaceous aerosols (Feng et al., 2005; Kirillova et al., 2014; Miyazaki et al., 2009). Because of its affinity with water,

* Corresponding author.
** Corresponding author.
E-mail addresses: cgtian@yic.ac.cn (C. Tian), yjchentj@tongji.edu.cn (Y. Chen).

http://dx.doi.org/10.1016/j.atmosenv.2016.08.078
1352-2310/

WSOC is absolutely responsible for altering the aerosol hygroscopicity, determining the particles acting as cloud condensation nuclei (CCN), and even for the formation of haze (Haque et al., 2016; Huang et al., 2006; Saffari et al., 2016; Sun et al., 2016; Wu et al., 2016). Generally, WSOC can be either directly emitted or formed in the atmosphere via the oxidation of the anthropogenic and biogenic volatile organic compounds (VOCs) (Kumagai et al., 2009). The latter was believed as the major formation pathway (Miyazaki et al., 2007), but rarely confirmed in field observation. Of VOCs involved in WSOC, aromatic compounds (Odum et al., 1997) and isoprene (Kroll et al., 2005; Limbeck, 2003) were deemed, respectively, as the primary anthropogenic and biogenic species. However, despite of the abundance and significance of WSOC in the atmosphere, there remains considerable uncertainty regarding the source and formation of WSOC (Park et al., 2011), especially in the areas with rapid economic growth and high population density.

The Bohai Rim, as the third largest economic zone in China (Xin et al., 2011), is located at the northern China around Bohai Sea and comprises Beijing and Tianjin municipalities as well as part of Hebei, Liaoning and Shandong province. In the past decades, it has experienced significant urbanization, land use change, and is potentially moving towards more serious carbonaceous aerosol pollution (Wang et al., 2014a; Zong et al., 2015). For example, a well study investigated the organic carbon precipitation elaborately and showed total carbon deposition flux could be up to 3.2 g C m^{-2} yr^{-1} in North China, greatly affecting the ecosystem (Pan et al., 2010). Considering the critical role of WSOC in the aerosol pollution, a certain amount of researches about its source and formation have been carried out by various methods, such as PMF modeling and traces (Du et al., 2014; Huang et al., 2006), in this region. However, significant difference was found from previous assessments mainly due to the particularly complicated source of WSOC (Pan et al., 2010). Fortunately, radiocarbon (^{14}C) measurement provides a chance to unambiguously differentiate biomass versus fossil sources for WSOC depending on its principle that the radioisotope has become extinct in fossil fuel carbon, while non-fossil carbon sources contain the contemporary or near contemporary radiocarbon level (Szidat et al., 2004). As a powerful technique, this method has been applied to the source apportionment of WSOC in south or big city of China. For example, recent studies found that 67% of WSOC in Guangzhou winter was derived from non-fossil fuel source (Liu et al., 2014); contemporary carbon accounted for 87% of WSOC in Hainan Island (Zhang et al., 2014c). While available information about WSOC source in North China, especially in Bohai Rim, was extremely limited.

Until now, a number of researches have indicated monitoring data from a background area could be used to assess the source apportionment of regional pollution (Liu et al., 2013; Schwarz et al., 2016; Squizzato et al., 2016). Furthermore, WSOC usually has higher value in background sites, also was found a greater contribution to OC during summer than winter (Park et al., 2011). Thus the information on the relative abundance of WSOC in background sites in summer can provide vital insight into the source and formation of WSOC. In this study, we collected fine particulate matter ($PM_{2.5}$) samples in summer, 2013 at the Yellow River Delta (YRD), North China for WSOC exploration about the factors affecting source and the formation. The objectives of this study are (1) to quantify the regional-scale concentration burden and temporal variation of WSOC, (2) to explore the formation mechanisms of WSOC and its influence factors, (3) to distinguish the anthropogenic source signals of WSOC based on the chemical composition of aerosols, (4) to assess the source apportionment of WSOC based on the CPF model and ^{14}C measurement.

2. Materials and methods

2.1. Sampling campaign

As shown in Fig. 1, the sampling site is located in the Yellow River Delta Ecological Research Station of Coastal Wetland (37°45′N, 118°59′E), Chinese Academy of Sciences, where no obvious anthropogenic emission source nearby. Yellow River Delta (YRD) is a regional background receptor site in the Bohai Rim, which is influenced by seasonally air pollution outflows from Beijing, Tianjin and Hebei (BTH) and Shandong, Anhui and Jiangsu province (SAJ) under the East winter and summer monsoon. The detailed information of the site has been described in our previous study (Zong et al., 2015). $PM_{2.5}$ samples were collected by a Tisch high volume sampler at a flow rate of 1.13 m^3 min^{-1}, from 29 May to 1 July 2013. The quartz fiber filters used were preheated at 450 °C for 6 h in muffle furnace to remove the impurity. The sampling procedure was derived into two time-resolutions (12 h & 6 h), of which the 12 h sample was collected from 6:00 to 18:00 (day time) and from 18:00 to 6:00 (night time) the next day, the 6 hourly sampling was from 6:00 to 12:00, 12:00 to 18:00, 18:00 to 24:00, and 24:00 to morrow 6:00, respectively. Overall, 76 samples were collected during the sampling period. After sampling, filters were folded, wrapped in aluminum foil, sealed in airtight plastic bags, and then stored in refrigerator (−20 °C) until analysis to prevent evaporation of volatile components. In addition, blank samples were collected to subtract possible contamination occurring during or after sampling.

2.2. Gravimetric weighing

Before and after each sampling, the quartz fiber filters were through a 24-h equilibration of 25 °C and 39% relative humidity,

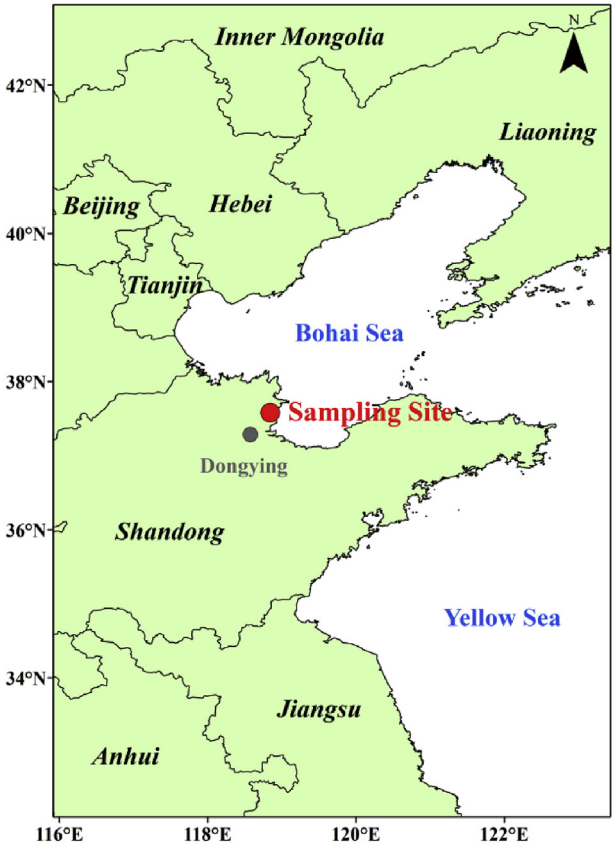

Fig. 1. The location of sampling site in Yellow River Delta, North China.

and then weighed by a Sartorius MC5 electronic microbalance with a ±1 μg sensitivity. Each filter was weighed for at least three times, the difference among three repeated weighing should be less than 10 μg for a blank filter and 20 μg for a sampled filter, respectively. The $PM_{2.5}$ concentration of each sample was equal to the weight difference before and after sampling divided by the sampled air volume.

2.3. Chemical analysis

Organic carbon (OC) and elemental carbon (EC) were analyzed by a Desert Research Institute (DRI) Model 2001 Carbon analyzer (Atmoslytic Inc., Calabasas, CA) following the Interagency Monitoring of Protected Visual Environment (IMPROVE_A) thermal/optical reflectance (TOR) protocol (Chow et al., 2007), which has been described in detail in our pervious study (Zong et al., 2015). For the measurements of WSOC and ionic species, briefly, one punch with 47 mm diameter was cut off from quartz fiber filters, and then was subjected to Milli-Q water. Samples were ultrasonically extracted for 20 min, and the extracts were filtered. Concentration of WSOC was determined by using a total carbon analyzer (TOC-VCPH, Shimadzu Corp., Kyoto Japan) with a detection limit < 0.01 ng ml^{-1} and error < 1.5%. Besides, water-insoluble organic carbon (WIOC) was quantified by OC given by TOR protocol subtracting WSOC. Anions (Cl^-, SO_4^{2-},NO_3^-) and cations (Na^+, K^+, Ca^{2+}, Mg^{2+}) were measured by the ion chromatograph (Dionex ICS3000, Dionex Ltd., America) based on the analysis method (Shahsavani et al., 2012). The detection limit of water-souble ions was 10 ng ml^{-1} with the error <5%. On the other hand, another punch with 47 mm diameter was induced acid digestion for heavy metal measurement. The concentration of metal elements (Cd, V, Cr, Mn, Fe, Ni, Cu, Zn, As, Pb) in aerosols was estimated by means of the inductively coupled plasma coupled with mass spectrometer (ICP-MS of ELAN DRC II type, Perkin Elmer Ltd., Hong Kong) on the basis of the standard method (Wang et al., 2006) with a detection limit < 0.01 ng ml^{-1} and error < 5%. It was noted that OC, EC, WSOC, ions, metal elements concentration in this study were all blank-corrected by subtracting the average field blank value.

2.4. Radiocarbon measurement

As mentioned above, about 20 ml Milli-Q water was used to extract the 47 mm diameter punch for WSOC. After filtration, the WSOC solution was further frozen in a 40 ml glass vial and then freeze-dried to dryness at −40 °C for 24 h by a freeze drier. The WSOC residue was re-dissolved with 0.5 ml ultra-pure water, and then transferred to a pre-combusted quartz tube to be also placed in the freeze dryer. Thereafter, the quartz tube was combusted at 850 °C converting WSOC into CO_2, which will be cryo-trapped, quantified manometrically, sealed in a quartz tube and reduced to graphite at 600 °C using zinc with iron (200 mg, Alfa Asear, 1.5–3 mm, 99.99%) catalyst 34 for accelerator mass spectrometry (AMS) target preparation (Zhang et al., 2014b). The preparation of graphite targets for AMS analysis was performed using the graphitization line at the Guangzhou Institute of Geochemistry, CAS. The determination of the isotopic ratio in the graphite samples was determined through NEC compact AMS at Peking University. Generally, ^{14}C result is expressed as fraction of modern carbon (f_m). It is larger than 1 due to the nuclear bomb and declines steadily from 1950s, which needs correction for the time period between 1950 and the year of measurement. So f_m values reported here were corrected as fraction of contemporary carbon (f_c) with the conversion factors of 1.10, 1.06 for EC and OC (including WSOC and WIOC), respectively (Levin et al., 2010; Mohn et al., 2008). In addition, isolated carbon amounts in this study were between 66.32 and 155.51 μg, while WSOC and WIOC in the blank samples only accounted for 0.91% and 1.11%, respectively. Thus, the blank interference for f_m was very small and was ignored (Liu et al., 2014).

2.5. Data analysis methods

2.5.1. Air trajectory generation

Backward trajectories, generated by the hybrid single-particle Lagrangian integrated trajectory (HYSPLIT) model, were used to assess the passing areas of air masses encountered during the sampling time (Liu et al., 2014; Zhang et al., 2014c; Zong et al., 2015). The model was available on the National Oceanic and Atmospheric Administration Air Resource Laboratory website (www.arl.noaa.gov/ready/hysplit4.html). In this paper, backward trajectories (72-h) were generated with 6 h time interval for air masses starting from the sampling site at 500 m above ground level.

2.5.2. Calculation of sea-salt source

Sea salt is usually calculated by the Na^+ or Cl^- (Zhang et al., 2013). However, Cl^- may be not suitable here because of its vast additional anthropogenic source. In this study, the average concentration of Na^+ was 0.29 μg m^{-3}, and then the concentration of sea-salt (ss) Cl^- was 0.52 μg m^{-3} according to the mass rations (1.80) in seawater (Ni et al., 2013). But the virtual value was 0.96 μg m^{-3}, which was much higher than the former. As a consequence, sea salt was achieved by the Na^+. On the basis of mass rations in seawater, the major sea-salt (ss) fraction of Mg^{2+}, K^+, Ca^{2+}, SO_4^{2-}, Cl^- were calculated by using the concentration of Na^+ multiplied by the factors 0.12, 0.036, 0.038, 0.252 and 1.80, respectively (Ni et al., 2013).

3. Results and discussion

3.1. Regime and intraday fluctuation of WSOC in summer

Table 1 lists the statistical values of OC, WSOC and WIOC in YRD during the sampling period. Overall, the level of WSOC ranged from 0.03 to 14.56 μg m^{-3} with an average value of 3.09 ± 2.45 μg m^{-3}, representing 56.39% of OC. The concentration was much lower than that in some urban area in China, such as Beijing (6.7 ± 4.4 μg m-3) (Du et al., 2014), Shanghai (5.8 ± 4.2) (Pathak et al., 2011), while was comparable to some typical cities abroad (Kumagai et al., 2009; Park et al., 2011). The proportion of WSOC in OC was higher than that of WIOC (43.61%), indicating WSOC was the major component of the OC in YRD. Parallel phenomenon was found in the observation of Kanto plain (Kumagai et al., 2009), Gwangju (Park et al., 2013) and so on. In addition, WSOC/OC ratio can also be used to assess the photochemical aging of organics, especially for the long-range transported aerosols (Kumagai et al., 2009). Compared with some urban regions in China, such as Shanghai (0.35), Guangzhou (0.32), Lanzhou (0.40) (Pathak et al., 2011), the WSOC/OC ratio was relative higher, suggesting organic aerosol in YRD was aged and mainly transported from other source regions. This was consistent with the regional background nature of our sampling site. The observed ratio in this study was similar to those reported in other background areas. For example, it was reported that 41%–75% of organic carbon was water-souble in Sapporo, North Japan (Agarwal et al., 2010); 45%–75% organic carbon was contributed by WSOC in Amazonia, which was largely due to the biomass burning (Mayol-Bracero et al., 2002).

Statistical values of OC, WSOC and WIOC in day time and night time was also provided in Table 1. Obviously, the concentrations of WSOC and WIOC in day time were higher than those in night time. However, there were no significant differences between the ratios of WSOC/OC, and WIOC/OC in day time and night time. The average

Table 1
The statistical information of OC, WSOC and WIOC in YRD with the unit of μg m^{-3} except for that of ratios. It was noted that high intensity collection in 6 h interval was conducted during 1st 18:00 to 4th 18:00 (First period) and 18th 18:00 to 21st 18:00 (Second period) in June. FBN, FAN and FBM, FAM refer to 6:00–12:00, 12:00–18:00 and 18:00–24:00, 24:00-morrow 6:00, respectively, in the first period; The same situation of SBN, SAN and SBM, SAM for the second period.

	OC	WSOC	WIOC	WSOC/OC	WIOC/OC
Day and Night (6:00-morrow 6:00)	5.48 ± 3.65	3.09 ± 2.45	2.39 ± 1.78	0.56 ± 0.15	0.44 ± 0.18
Day (6:00–18:00)	6.86 ± 4.11	3.82 ± 2.77	3.03 ± 2.11	0.56 ± 0.11	0.44 ± 0.16
Night (18:00-morrow 6:00)	4.20 ± 2.62	2.41 ± 1.90	1.79 ± 1.13	0.57 ± 0.17	0.43 ± 0.22
Day/Night	1.63	1.59	1.69	–	–
FBN (6:00–12:00)	6.84 ± 3.59	4.13 ± 2.15	2.71 ± 2.19	0.60 ± 0.09	0.40 ± 0.15
FAN (12:00–18:00)	11.10 ± 3.85	7.28 ± 1.65	3.82 ± 3.61	0.66 ± 0.09	0.34 ± 0.13
FBN/FAN	0.63	0.60	0.66	–	–
FBM (18:00–24:00)	4.52 ± 2.07	2.56 ± 1.56	1.96 ± 0.77	0.57 ± 0.04	0.43 ± 0.04
FAM (24:00-morrow 6:00)	4.56 ± 3.30	2.84 ± 3.40	1.72 ± 0.98	0.62 ± 0.03	0.38 ± 0.04
FBM/FAM	0.97	0.79	1.31	–	–
SBN (6:00–12:00)	4.00 ± 1.35	2.49 ± 1.28	1.51 ± 0.50	0.62 ± 0.10	0.38 ± 0.15
SAN (12:00–18:00)	6.15 ± 2.59	3.54 ± 2.01	2.61 ± 0.74	0.58 ± 0.12	0.42 ± 0.06
SBN/SAN	0.65	0.70	0.58	–	–
SBM (18:00–24:00)	1.63 ± 1.31	0.6 ± 0.77	1.03 ± 1.12	0.37 ± 0.40	0.63 ± 0.62
SAM (24:00-morrow 6:00)	1.79 ± 1.06	1.29 ± 0.94	0.5 ± 0.17	0.72 ± 0.61	0.28 ± 0.06
SBM/SAM	0.91	0.47	2.06	–	–

day-to-night (D/N) ratios for OC and WSOC, WIOC were 1.63, 1.59 and 1.69, respectively, also exhibiting no different characteristic ($p > 0.05$). This implied their emission sources were similar and their formation pathways were almost stable during day and night time. The relative higher concentration in day time suggested the stronger emissions of these species or their precursors at that time, mainly ascribing to the human activities (Kumagai et al., 2009). In order to further explore the fluctuation reason of WSOC in day and night time, two high intensity collections in 6 h interval were conducted during 1st 18:00 to 4th 18:00 and 18th 18:00 to 21st 18:00 in June 2013. As mentioned in section 2.1, the 6 h interval included four types of time period: 6:00–12:00 (BN), 12:00–18:00 (AN), 18:00–24:00 (BM), 24:00-morrow 6:00 (AM). Generally, the concentration of WSOC increased gradually from BM stage and reached peak at the next AN stage. While concentration of WIOC decreased in the AM stage compared with BM stage, and increased again from next BN to AN stage. WIOC usually better represents primary OC emitted directly from combustion, whereas WSOC is a major portion of biomass-burning OC and second OC (Zhang et al., 2014c). So based on the variation of WIOC, the conclusion that strength of the emission source increased from BM to AN stage, but declined distinctly in AM stage was draw. While the increase of WSOC in the AM stage was attributed to the stronger second formation from its precursor under stable atmospheric condition (Kroll et al., 2005), which was further proved by the higher WSOC/OC ratio in AM stage compared with that of WIOC. In addition, the contaminant burdens of OC, WSOC and WSOC during the first period (1st 18:00 to 4th 18:00) were higher than those in the second period (18th 18:00 to 21st 18:00). This was ascribed to that the air masses in first period was from south source region and encountered agricultural field burning, nevertheless, winds blowing from the clear sea presumably diluted and dispersed the air pollutants, resulting in relative lower concentrations in the second period. Detailed discussion can be found in our previous study (Zong et al., 2015). The great difference of the two periods could provide vital information about the WSOC source region in YRD.

3.2. Secondary nature of WSOC and its relationship with aerosol acidity

WSOC consists of various secondary groups, such as alcohols, carbonyls, dicarboxylic acids and considerable photochemical production (Snyder et al., 2009). For better understanding of the secondary nature of WSOC observed in YRD, its relationship between secondary organic carbon (SOC) was explored. The estimate of SOC was determined using the EC-tracer method (Pathak et al., 2011):

$$SOC = OC - (OC/EC)_{prim} \times EC \quad (1)$$

where $(OC/EC)_{prim}$ was the ratio of OC to EC for primary emissions. Here, the minimum OC/EC was adopted as the $(OC/EC)_{prim}$ and this usage has been cited in various studies (Du et al., 2014). Consequently, the mean estimated concentration of SOC was 2.41 μg m^{-3}, accounting for 77.90% of WSOC on average. It was not surprising that the percent was not 100%, because some WSOC such as amino acids, urea etc. were not SOC (Fang et al., 2015). The correlation analysis between WSOC and SOC was examined and shown in Fig. 2. WSOC and SOC exhibited a significant linear relation ($r = 0.82$, $p < 0.01$), which greatly proved the secondary nature of WSOC (Rengarajan et al., 2011). Additionally, Secondary inorganic ions (SIA) consist of SO_4^{2-}, NO_3^- and NH_4^+ seen in Table S1. Among them, SO_4^{2-} is usually transformed from SO_2 via gas-phase, heterogeneous, or multiphase processes (Pan et al., 2016); NO_3^- is converted from the reactive oxidized nitrogen compounds and NH_4^+ is formed from NH_3 through neutralization of atmospheric acids (Hu et al., 2014). These conversion processes demonstrated the secondary characteristic of SIA. In this case, correlation of WSOC with SIA was also investigated in this study (Fig. 2). The correlation coefficient was slightly lower than that of SOC, but was still around 0.7, also indicating a great correlation between WSOC with SIA. In general, a good correlation possibly suggested a similar source or formation pathway, so the relative lower correlation coefficient between WSOC and SIA could be ascribed to their different sources. For example, NH_4^+ arises mainly from animal husbandry and synthetic fertilizers (Dawson et al., 2014), which shares significant difference with WSOC. It was found that coal combustion, the main source of SO_2, was not likely an important source for WSOC (Wahlin et al., 2006). Similar conclusion was also conducted in Beijing from a yearlong study (Du et al., 2014).

As discussed above, WSOC mainly consisted of SOC, of which the formation was greatly influenced by particle phase acidity via heterogeneous oxidation processes in the atmosphere (Pathak et al., 2011). The theory has been proved in the laboratory

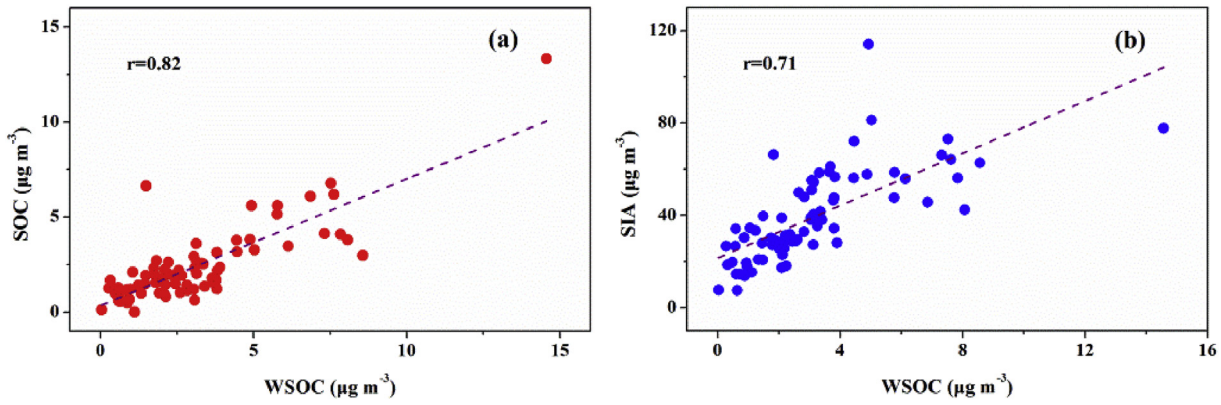

Fig. 2. The relationship between WSOC and SOC (a), WSOC and SIA (b). WSOC and SOC exhibited a significant linear relation ($r = 0.82$, $p < 0.01$), while correlation coefficient between WSOC and SIA was slightly lower.

chamber research. Studies have shown that the mass of SOC and the acidity of laboratory-generated aerosol exhibited a linear relationship (Surratt et al., 2007). In this study, the relationship between WSOC and acidity was explored for the purpose of providing the direct evidence for enhanced WSOC formation at high level of acidity in the field-based research. The acidity of atmosphere aerosols (H^+) was estimated using the difference between the equivalence concentrations of anions and cations as expressed below:

$$\left[H^+\right] = [Anion] - [Cation] \quad (2)$$

Apparently, if $H^+ < 0$, the anions were fully neutralized by cations; and if $H^+ > 0$, the aerosols were acidic. During the sampling period, the value of H^+ was highly variable, ranging from −0.03 μmol m^{-3} to 1.64 μmol m^{-3}, with a mean value of 0.38 μmol m^{-3}. It was slightly higher than that in some big cities, while comparable to that at a rural site in Beijing (Pathak et al., 2009, 2011). This was mainly due to the low concentration of NH_4^+ and the high concentrations of SO_4^{2-} and NO_3^- observed in these background regions. NH_4^+ was associated with SO_4^{2-} firstly, and any excess was with NO_3^- and Cl^- (Hu et al., 2014). The average value of $[NH_4^+]/[SO_4^{2-}]$ during the sampling campaign was 1.18, suggesting the most samples had no enough NH_4^+ to neutralize SO_4^{2-} in YRD, thus H^+ may be mainly in the form of HNO_3 or HCl.

The relationship between WSOC and acidity was explored by the following two methods. Firstly, the 25th and 75th percentile of H^+ were got by the means of statistic analysis, then the concentrations of WSOC and the WSOC/OC ratios that corresponding to higher H^+ values (higher than 75th) and lower values (less than 25th) were compared. This comparison method was usually adopted in mathematical statistics (Zhang et al., 2014a). When H^+ was higher than 0.53 μmol m^{-3} (75% of the total values), the corresponding average concentration of WSOC was 5.35 μg m^{-3} with a WSOC/OC value of 0.59. While the mean value of WSOC/OC for the lower H^+ (less than 25th) could drop to 0.49 and the WSOC concentration was 1.32 μg m^{-3}, which was significant ($p < 0.01$) lower than that of former. This implied acidity could promote the formation of WSOC. Secondly, Fig. 3 illustrated the time series of characteristics of WSOC and H^+, also implying a positive correlation between them, and the regression equation was $WSOC = 5.58\ H^+ + 0.989$. The slope suggested that an increase of H^+ by 0.1 μmol m^{-3} would increase 0.56 μg m^{-3} WSOC in the aerosols, which was approximately half of that (1.2 μg m^{-3}) observed in the Changdao Island (Feng et al., 2012). This was mainly due to the much higher level of acidity in YRD compared with Changdao

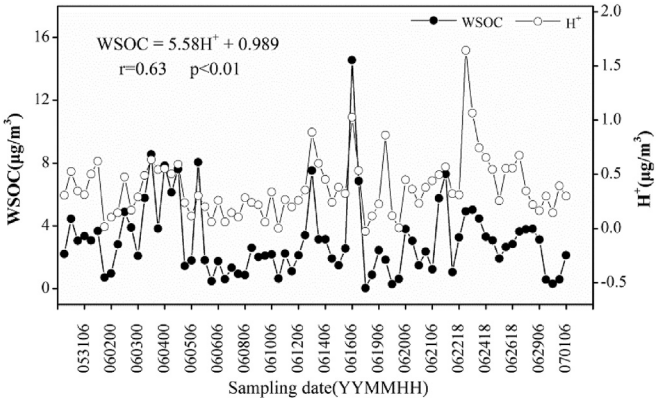

Fig. 3. Time series of the characteristics of WSOC and H^+ observed in YRD.

Island. Meanwhile, the intercept of 0.99 may indicate that part of WSOC was unrelated to the acidity. To sum up, it is postulated that the increase of WSOC could be linked to the increase of acidity in the particle phase on the basis of the observation in this study.

3.3. Anthropogenic nature of WSOC based on $PM_{2.5}$ source signals

The variety of species in $PM_{2.5}$ (Table S1) could provide vital information about the source of aerosols. We have proved that open biomass burning contributed greatly to aerosols on the basis of OC and EC (Zong et al., 2015). In this study, the concentration of K^+, usually treated as the marker of biomass burning, was relative higher compared with other regions (Zhang et al., 2013), further supporting our previous viewpoints. For figuring out the anthropogenic source of WSOC, correlation coefficient of semidiurnal WSOC with major no-carbonaceous species in $PM_{2.5}$ was conducted as displayed in Table 2. Generally, high correlations of species in $PM_{2.5}$ suggested their strong co-emission or common sources. Here, correlation coefficient exceeding 0.6 ($p < 0.01$) was considered as significant correlations (Kim et al., 2016). So NO_3^-, SO_4^{2-}, K^+, Cu and Zn with correlation coefficient of 0.76, 0.64, 0.80, 0.66 and 0.68, respectively, demonstrated that they shared common sources with WSOC, while other species were not in YRD. These species usually derive from anthropogenic sources (Zhang et al., 2014a). However, SO_4^{2-} and K^+ are also important composition of sea salt, and the sampling site was on the seafront, which may hold back the confirmation of their anthropogenic source. Based on the estimated method in section 2.5.2, the species levels from sea salt (ss) could

Table 2
Correlation coefficient of major no-carbonaceous species in $PM_{2.5}$ with WSOC.

Species	Correlation coefficient with WSOC	Sig.	Species	Correlation coefficient with WSOC	Sig.
Cl^-	0.11	$p > 0.05$	V	−0.05	$p > 0.05$
NO_3^-	0.76	$p < 0.01$	Cr	−0.04	$p > 0.05$
SO_4^{2-}	0.64	$p < 0.01$	Mn	0.43	$p < 0.01$
Na^+	0.32	$p < 0.05$	Fe	0.28	$p < 0.05$
NH_4^+	0.56	$p < 0.01$	Ni	0.06	$p > 0.05$
K^+	0.80	$p < 0.01$	Cu	0.66	$p < 0.01$
Mg^{2+}	0.18	$p < 0.05$	Zn	0.68	$p < 0.01$
Ca^{2+}	0.25	$p < 0.05$	As	0.15	$p > 0.05$
Cd	0.32	$p < 0.05$	Pb	0.25	$p < 0.05$

be achieved by Na^+ as a tracer, and then the amount of non sea salt (nss) of species can be achieved. According to the calculation, nss-SO_4^{2-}, nss-K^+ accounted for 99.64%, 99.44%, respectively, of their corresponding total concentration. The marked high proportion of nss-emission for SO_4^{2-}, K^+ certified their significant anthropogenic source and their sea salt source could be ignored. Nss-K^+ was an excellent sign of biomass burning, while the fossil fuel combustion was generally featured by high content of nss-SO_4^{2-}, NO_3^-, Zn and Cu (Zhang et al., 2013). Thus WSOC in YRD was mostly influenced by biomass burning and fossil fuel combustion. The result was consistent with many researches conclusions about the source of WSOC in various regions (Mayol-Bracero et al., 2002; Weber et al., 2007).

Likewise, multiple linear regressions were applied to further explore the relationship between WSOC and NO_3^-, nss-SO_4^{2-}, nss-K^+, Cu, Zn. After standardization, the equation between concentration of WSOC and factors was expressed as:

$$C(WSOC) = 0.67x_1 - 0.54x_2 + 0.75x_3 + 0.19x_4 + 0.26x_5 \quad (3)$$

($p < 0.01$, x_1, x_2, x_3, x_4, x_5, stand for NO_3^-, nss-SO_4^{2-}, nss-K^+, Cu, Zn, respectively). Fig. S1 displayed the scatter plot between observed WSOC and expected WSOC with significant correlation, suggesting the effectiveness of equation. Therefore, NO_3^-, nss-K^+, Cu, Zn had positive correlation with WSOC, while the correlation between WSOC and nss-SO_4^{2-} was negative. This indicated that, apart from influence of co-emission with high correlation species, nss-SO_4^{2-} may be counteractive to the formation of WSOC in YRD. It may be attributed to the competitive relation between VOCs and SO_2 in oxidation environment. In addition, field and laboratory studies have shown that NO_x acted as a catalyst and could promote the conversion of SO_2 to SO_4^{2-} in the atmosphere (He et al., 2014; Wang et al., 2014b), thus the correlation (0.64) between WSOC and nss-SO_4^{2-} could be mainly ascribed to the close relationship between SO_4^{2-} and NO_3^- (Text S1). In particular, NO_3^- forms in the atmosphere when OH radicals or O_3 reacts with NO_x. The latter is usually emitted from high temperature combustion processes, such as vehicle and industrial facilities, which are also important sources for Zn and Cu in aerosols (Tan et al., 2014). It was found that atmospheric Zn not only emitted from vehicle direct exhaust, but from lubricating oil additives, tyre and brake abrasion (Duan and Tan, 2013). The phenomenon that traffic-generated aerosol particles were rich in Cu, Zn, Mo, and Sb was also observed (Wahlin et al., 2006). Besides, NO_3^-, Zn and Cu were always treated as vehicle tracer in the Positive Matrix Factorization analysis (Zhang et al., 2013). Hence, the closed relationship between WSOC and NO_3^-, Zn and Cu may prove the great proportion of vehicle emission in the fossil fuel combustion. Zn and Cu had higher degree of contamination compared with other metal elements according to the Enrichment factor (EF) analysis (Test S2), which also implied vehicle emission was an important source for aerosols in YRD. However, it was noteworthy that correlation between WSOC and nss-K^+ was the most significant among the signals, suggesting biomass burning might be the most important source of WSOC in YRD. This would be further confirmed by radiocarbon measurement in section 3.4.

3.4. Source apportionment of WSOC

Conditional probability function (CPF) analysis can be used to investigate the influence of different source regions on target species at the receptor site, and was adopted here to assess WSOC in YRD. This method has been described in detail in another study (Park et al., 2011). Briefly, CPF estimates the probability that a given source contribution from a given wind direction will exceed a predetermined threshold criterion. It has been widely used to analyze the source impacts from varying wind direction in the source apportionment researches (Ogulei et al., 2005; Park et al., 2011). In this study, the average WSOC flux (concentration × speed), which could be more representative for source information, coupled with wind direction were employed to calculate the probability. Wind speed and direction were obtained from a Three-Dimensional Ultrasonic Anemometer (CSAT-3, Campbell Scientific, Logan, USA). The CPF analysis was expressed as the following equation:

$$CPF_{\Delta\theta} = m_{\Delta\theta}/n_{\Delta\theta} \quad (4)$$

where $m_{\Delta\theta}$ was the number of occurrences from wind sector $\Delta\theta$ that exceed the threshold criterion, while $n_{\Delta\theta}$ was the total number of date point from the same wind sector. Here, $\Delta\theta$ was set at 15°, and 75 percentile of WSOC flux was employed as the threshold criterion for defining the directionality of the sources. It should be noted that the WSOC flux dates corresponding to wind speeds (<1 m s^{-1}) were excluded because the direction of a sources was not well determined at low wind speed (Park et al., 2008). Fig. 4 displayed the CPF plot of WSOC flux, describing the conditional probability values of wind direction, and higher values indicated more likely the location of sources. Obviously, the significant contribution of WSOC occurred when the wind came from southerly (135–195°) and northwesterly (285, 345°) directions. From the location of sampling site (Fig. 1), the northwesterly air mass was mostly from Beijing-Tianjin-Hebei (BTH) region, while the southerly was mainly derived from Shandong-Anhui-Jiangsu (SAJ) area. Based on the results of CPF, and in order to further confirm the source of WSOC, ^{14}C measurement was conducted to evaluate the source apportionment of WSOC from the two directions.

For better achieving our purpose by a few radiocarbon samples due to the extensive cost, two combined samples were collected from two perfect synoptic processes, respectively, as shown in Fig. 5. The first combined sample (C1) was merged by four six-hour samples collected on the 3rd, June, when air masses of synoptic processes were derived from the southerly direction (SAJ region). Similarly, the other sample (C2) was combined by two twelve-hour

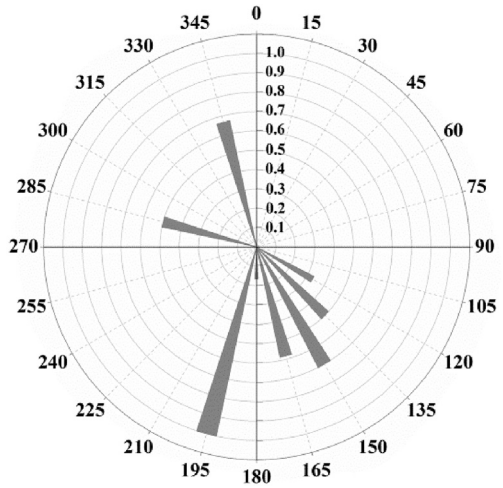

Fig. 4. CPF plots of WSOC flux (μg m^{-2} s^{-1}) for the 75th percentiles. Significant contribution of WSOC occurred when the wind came from southerly and northwesterly directions.

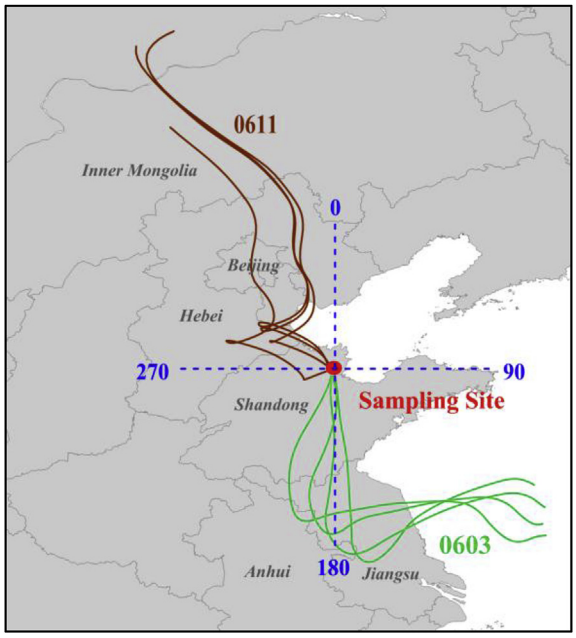

Fig. 5. 72-h back trajectories of the two merged samples. C1 was collected on the 3rd, June, reflecting the source signal from SAJ region; C2 was collected on the 11th, June, showing the source pattern from BTH region.

samples collected on 11th, June, when the air trajectories came from northwest (BTH region). The concentrations of WSOC and WSOC/OC ratios in C1 and C2 were compared with those of total samples in corresponding directions, respectively, by mean test. Results showed that the concentration of WSOC and WSOC/OC ratio in C1 were insignificantly different from those of total samples from southerly direction at a 95% significant level, and the same situation applied to C2, indicating their perfect representative capabilities for further radiocarbon analysis. Thus, we can see that C1 reflected the source signal from SAJ region and C2 showed the source pattern from BTH region.

Table 3 lists the statistical values about C1 and C2 selected for ^{14}C measurement. The average f_c value for WSOC was 0.57 ± 0.01, indicating biogenic and biomass burning (B&B) was the major source for WSOC at the YRD in summer. While f_c(WIOC) and f_c(EC) were 0.69 ± 0.02, 0.54 ± 0.03, respectively (Zong et al., 2015), implying EC was more contributed by fossil source. Similar results were found in some background sites, such as Ningbo (Liu et al., 2013) and Hainan Island (Zhang et al., 2014c). However, the contribution of B&B to WSOC was lower than that of WIOC, which was different from other regions (Liu et al., 2014). As mentioned above, WIOC better represented primary organic carbon, whereas WSOC was a major portion of SOC derived from anthropogenic and biogenic volatile organic compounds (VOCs) (Zhang et al., 2014c). Thus fossil fuel may have a greater impact on VOCs, the precursor of WSOC, compared with WIOC in YRD during the sampling period.

The concentration of WSOC and WSOC/OC ratio was 5.06 ± 2.78 μg m^{-3} and 0.49 ± 0.07, respectively, during the southerly synoptic process. While the concentration of WSOC fell to 1.67 ± 0.79 μg m^{-3}, and WSOC/OC ratio rose to 0.63 ± 0.04 for the northerly synoptic stage. The decreasing tendency of concentration was consistent with that of OC, EC and WIOC, which could be caused by the increase of wind speed (from 2.09 to 4.51 m s^{-1}). However, the rise of WSOC/OC ratio could indicate the different source characteristic of WSOC from other carbonaceous species. It was confirmed by radiocarbon results of the two merged samples. The f_c(WIOC) and f_c(EC) on 3rd, June were 0.74 ± 0.02 and 0.59 ± 0.03, respectively, which were higher than that (0.63 ± 0.03 and 0.48 ± 0.03) on 11th, June. This implied that the influence of B&B on primary carbonaceous species, such as WIOC and EC, in SAJ region was more significant than that of BTH region. Interestingly, the f_c(WSOC) of C1 was 0.54 ± 0.01, lower than 0.59 ± 0.01 of C2, which was contrary to the tendency of WIOC and EC but consistent with WSOC/OC ratio. The adverse tendency of f_c(WSOC) indicated the impact of fossil fuel on WSOC in SAJ region was higher than that of BTH region, which consisted with the relative higher proportion of nss-K^+ in C2 (3.49 ± 0.5%) compared with C1 (2.01 ± 0.1%). Besides, the higher NO_3^-/nss-SO_4^{2-} ratio, an indicator of the importance of mobile vs. stationary sources (Liu et al., 2014), suggested a larger proportion of vehicle emission in fossil fuel in SAJ. It was not surprise because except for the acknowledged high level of vehicle emissions in BTH region, there were also many vehicle sources existing in SAJ region. For example, the car ownership in Shandong and Jiangsu province had ranked the first and third, respectively in China (Yearbook, 2014), exhibiting great vehicle pollution. To sum up, the contribution of fossil fuel, mainly vehicle exhaust, to WSOC was still important, although biomass burning has been identified as a major source for carbonaceous species in North China in summer (Zhao et al., 2012). It was consistent with that discussed above in section 3.3. Not only WSOC showed a significant relationship with nss-K^+, but also correlated well with high contents of NO_3^-, Zn and Cu, typical indicators of vehicle exhaust.

Table 3
The important information about combined sample C1 and C2.

	C1	C2	Unit	
OC	10.06 ± 5.00	2.67 ± 0.41	μg m^{-3}	Zong et al., 2015
EC	4.60 ± 3.07	0.80 ± 0.20	μg m^{-3}	Zong et al., 2015
WIOC	5.00 ± 2.28	1.00 ± 0.38	μg m^{-3}	Zong et al., 2015
WSOC	5.06 ± 2.78	1.67 ± 0.79	μg m^{-3}	This study
WSOC/OC	0.49 ± 0.07	0.63 ± 0.04	–	This study
f_c(WSOC)	0.54 ± 0.01	0.59 ± 0.01	–	This study
f_c(WIOC)	0.74 ± 0.02	0.63 ± 0.03	–	Zong et al., 2015
f_c(EC)	0.59 ± 0.03	0.48 ± 0.03	–	Zong et al., 2015
NO_3^-/nss-SO_4^{2-}	0.77 ± 0.11	0.61 ± 0.11	–	This study
nss-K^+/$PM_{2.5}$	2.01% ± 0.1%	3.49% ± 0.5%	–	This study
Wind direction	South	North	–	This study
Wind speed	2.09 ± 0.83	4.51 ± 0.55	m s^{-1}	This study

4. Summary and conclusion

Continuous measurement of WSOC was conducted at YRD, a background site in North China, from 29 May to 1 July 2013. Results showed that concentration of WSOC ranged from 0.03 to 14.56 μg m^{-3} with an average of 3.09 ± 2.45 μg m^{-3}, accounting for 56.39% of OC. The WSOC/OC ratio was relative higher compared with that of other regions in China. This proved organic aerosol was aged and the background characteristic of YRD. Generally, WSOC concentration increased gradually from BM stage and reached peak at next AN stage, however, WIOC decreased in the AM stage compared with BM stage, and increased again from next BN to AN stage. It can be seen emission source increased from BM to AN stage, but declined distinctly in AM stage, while the increase of WSOC in the AM stage was attributed to the stronger second formation from its precursor under stable atmospheric condition. The favorable relationship between WSOC and SOC implied the observed WSOC was mostly secondary formation product, greatly affected by aerosol acidity. WSOC correlated well with nss-K^+, nss-SO_4^{2-}, NO_3^-, Zn and Cu, suggesting that a major part of observed WSOC and/or its precursors was of biomass burning and fossil fuel combustion origin. Moreover, vehicle emission may make great proportion in the fossil fuel combustion.

Conditional probability function (CPF) analysis showed great contribution of WSOC occurred when the wind came from southerly (135–195°) and northwesterly (285, 345°) directions, namely SAJ region and BTH region, respectively. In order to further confirm the source of WSOC, two merged samples from the two directions were selected for radiocarbon analysis. Before analysis, mean test showed the concentration of WSOC and WSOC/OC ratio in the two combined samples were insignificantly different from those of the total samples from southerly and northerly direction at a 95% significant level, indicating their perfect representative capabilities for radiocarbon analysis. The radiocarbon measurements demonstrated the average value of f_c(WSOC) was 0.57 ± 0.01, implying biogenic and biomass burning (B&B) was the major source of WSOC at the YRD in summer. Fossil fuel contribution was also important, and vehicle emission may occupy a larger proportion in fossil fuel. To sum up, the source and formation information of WSOC confirmed in this study could give crucial implication for its control strategies in the North China.

Notes

The authors declare no competing financial interest.

Acknowledgment

This work was supported by the Natural Scientific Foundation of China (Nos. 41471413) and the CAS Strategic Priority Research Program (Nos. XDA11020402, XDB05030303 and XDB05040503). The authors gratefully acknowledge the National Oceanic and Atmospheric Administration's Air Resources Laboratory for providing the HYSPLIT transport model and the READY website (http://www.arl.noaa.gov/ready.html).

Appendix A. Supplementary data

Supplementary data related to this article can be found at http://dx.doi.org/10.1016/j.atmosenv.2016.08.078.

References

Agarwal, S., Aggarwal, S.G., Okuzawa, K., Kawamura, K., 2010. Size distributions of dicarboxylic acids, ketoacids, alpha-dicarbonyls, sugars, WSOC, OC, EC and inorganic ions in atmospheric particles over Northern Japan: implication for long-range transport of Siberian biomass burning and East Asian polluted aerosols. Atmos. Chem. Phys. 10, 5839–5858.

Chow, J.C., Watson, J.G., Chen, L.W.A., Chang, M.C.O., Robinson, N.F., Trimble, D., et al., 2007. The IMPROVE_A temperature protocol for thermal/optical carbon analysis: maintaining consistency with a long-term database. J. Air & Waste Manag. Assoc. 57, 1014–1023.

Dawson, M.L., Perraud, V., Gomez, A., Arquero, K.D., Ezell, M.J., Finlayson-Pitts, B.J., 2014. Measurement of gas-phase ammonia and amines in air by collection onto an ion exchange resin and analysis by ion chromatography. Atmos. Meas. Tech. 7, 2733–2744.

Du, Z., He, K., Cheng, Y., Duan, F., Ma, Y., Liu, J., et al., 2014. A yearlong study of water-soluble organic carbon in Beijing I: sources and its primary vs. secondary nature. Atmos. Environ. 92, 514–521.

Duan, J., Tan, J., 2013. Atmospheric heavy metals and Arsenic in China: situation, sources and control policies. Atmos. Environ. 74, 93–101.

Fang, T., Guo, H., Verma, V., Peltier, R.E., Weber, R.J., 2015. $PM_{2.5}$ water-soluble elements in the southeastern United States: automated analytical method development, spatiotemporal distributions, source apportionment, and implications for heath studies. Atmos. Chem. Phys. 15, 11667–11682.

Feng, J.L., Guo, Z.G., Zhang, T.R., Yao, X.H., Chan, C.K., Fang, M., 2012. Source and formation of secondary particulate matter in PM2.5in Asian continental outflow. J. Geophys. Res. Atmos. 117 (n/a-n/a).

Feng, Y., Wen, S., Chen, Y., Wang, X., Lu, H., Bi, X., et al., 2005. Ambient levels of carbonyl compounds and their sources in Guangzhou, China. Atmos. Environ. 39, 1789–1800.

Haque, M.M., Kawamura, K., Kim, Y., 2016. Seasonal variations of biogenic secondary organic aerosol tracers in ambient aerosols from Alaska. Atmos. Environ. 130, 95–104.

He, H., Wang, Y.S., Ma, Q.X., Ma, J.Z., Chu, B.W., Ji, D.S., et al., 2014. Mineral dust and NOx promote the conversion of SO2 to sulfate in heavy pollution days. Sci. Rep. 4.

Hu, G., Zhang, Y., Sun, J., Zhang, L., Shen, X., Lin, W., et al., 2014. Variability, formation and acidity of water-soluble ions in PM2.5 in Beijing based on the semi-continuous observations. Atmos. Res. 145–146, 1–11.

Huang, X.-F., Yu, J.Z., He, L.-Y., Yuan, Z., 2006. Water-soluble organic carbon and oxalate in aerosols at a coastal urban site in China: size distribution characteristics, sources, and formation mechanisms. J. Geophys. Res. 111.

Kim, H., Kim, J.Y., Jin, H.C., Lee, J.Y., Lee, S.P., 2016. Seasonal variations in the light-absorbing properties of water-soluble and insoluble organic aerosols in Seoul, Korea. Atmos. Environ. 129, 234–242.

Kirillova, E.N., Andersson, A., Tiwari, S., Srivastava, A.K., Bisht, D.S., Gustafsson, Ö., 2014. Water-soluble organic carbon aerosols during a full New Delhi winter: isotope-based source apportionment and optical properties. J. Geophys. Res. Atmos. 119, 3476–3485.

Kroll, J.H., Ng, N.L., Murphy, S.M., Flagan, R.C., Seinfeld, J.H., 2005. Secondary organic aerosol formation from isoprene photooxidation under high-NOxconditions. Geophys. Res. Lett. 32 n/a-n/a.

Kumagai, K., Iijima, A., Tago, H., Tomioka, A., Kozawa, K., Sakamoto, K., 2009. Seasonal characteristics of water-soluble organic carbon in atmospheric particles in the inland Kanto plain, Japan. Atmos. Environ. 43, 3345–3351.

Levin, I., Naegler, T., Kromer, B., Diehl, M., Francey, R.J., Gomez-Pelaez, A.J., et al., 2010. Observations and modelling of the global distribution and long-term trend of atmospheric 14CO(2). Tellus Ser. B Chem. Phys. Meteorol. 62, 26–46.

Limbeck, A., 2003. Secondary organic aerosol formation in the atmosphere via heterogeneous reaction of gaseous isoprene on acidic particles. Geophys. Res. Lett. 30.

Liu, D., Li, J., Zhang, Y., Xu, Y., Liu, X., Ding, P., et al., 2013. The use of levoglucosan and radiocarbon for source apportionment of PM(2.5) carbonaceous aerosols at a background site in East China. Environ. Sci. Technol. 47, 10454–10461.

Liu, J., Li, J., Zhang, Y., Liu, D., Ding, P., Shen, C., et al., 2014. Source apportionment using radiocarbon and organic tracers for PM2.5 carbonaceous aerosols in Guangzhou, South China: contrasting local- and regional-scale haze events. Environ. Sci. Technol. 48, 12002–12011.

Mayol-Bracero, O.L., Guyon, P., Graham, B., Roberts, G., Andreae, M.O., Decesari, S., et al., 2002. Water-soluble organic compounds in biomass burning aerosols over Amazonia - 2. Apportionment of the chemical composition and importance of the polyacidic fraction. J. Geophys. Res. Atmos. 107.

Miyazaki, Y., Kondo, Y., Han, S., Koike, M., Kodama, D., Komazaki, Y., et al., 2007. Chemical characteristics of water-soluble organic carbon in the Asian outflow. J. Geophys. Res. 112.

Miyazaki, Y., Kondo, Y., Shiraiwa, M., Takegawa, N., Miyakawa, T., Han, S., et al., 2009. Chemical characterization of water-soluble organic carbon aerosols at a rural site in the Pearl River Delta, China, in the summer of 2006. J. Geophys. Res. 114.

Mohn, J., Szidat, S., Fellner, J., Rechberger, H., Quartier, R., Buchmann, B., et al., 2008. Determination of biogenic and fossil CO2 emitted by waste incineration based on (CO2)-C-14 and mass balances. Bioresour. Technol. 99, 6471–6479.

Ni, T.R., Li, P.H., Han, B., Bai, Z.P., Ding, X., Wang, Q.W., et al., 2013. Spatial and temporal variation of chemical composition and mass closure of ambient PM10 in Tianjin, China. Aerosol Air Qual. Res. 13, 1832–1846.

Odum, J.R., Jungkamp, T.P.W., Griffin, R.R., Flagan, R.C., Seinfeld, J.H., 1997. The atmospheric aerosol-forming potential of whole gasoline vapor. Science 276, 96–99.

Ogulei, D., Hopke, P.K., Zhou, L., Paatero, P., Park, S.S., Ondov, J.M., 2005. Receptor modeling for multiple time resolved species: the Baltimore supersite. Atmos.

Environ. 39, 3751–3762.
Pan, Y., Wang, Y., Zhang, J., Liu, Z., Wang, L., Tian, S., et al., 2016. Redefining the importance of nitrate during haze pollution to help optimize an emission control strategy. Atmos. Environ. 141, 197–202.
Pan, Y.P., Wang, Y.S., Xin, J.Y., Tang, G.Q., Song, T., Wang, Y.H., et al., 2010. Study on dissolved organic carbon in precipitation in Northern China. Atmos. Environ. 44, 2350–2357.
Park, S.-S., Schauer, J.J., Cho, S.-Y., 2013. Sources and their contribution to two water-soluble organic carbon fractions at a roadway site. Atmos. Environ. 77, 348–357.
Park, S.S., Ko, J.M., Cho, S.Y., 2011. Investigation of possible sources of water-soluble organic carbon particles observed with an online monitoring system. Atmos. Environ. 45, 3257–3266.
Park, S.S., Lee, K.-H., Kim, Y.J., Kim, T.Y., Cho, S.Y., Kim, S.J., 2008. High time-resolution measurements of carbonaceous species in PM2.5 at an urban site of Korea. Atmos. Res. 89, 48–61.
Pathak, R.K., Wang, T., Ho, K.F., Lee, S.C., 2011. Characteristics of summertime PM2.5 organic and elemental carbon in four major Chinese cities: implications of high acidity for water-soluble organic carbon (WSOC). Atmos. Environ. 45, 318–325.
Pathak, R.K., Wu, W.S., Wang, T., 2009. Summertime PM2.5 ionic species in four major cities of China: nitrate formation in an ammonia-deficient atmosphere. Atmos. Chem. Phys. 9, 1711–1722.
Rengarajan, R., Sudheer, A.K., Sarin, M.M., 2011. Aerosol acidity and secondary organic aerosol formation during wintertime over urban environment in western India. Atmos. Environ. 45, 1940–1945.
Saffari, A., Hasheminassab, S., Shafer, M.M., Schauer, J.J., Chatila, T.A., Sioutas, C., 2016. Nighttime aqueous-phase secondary organic aerosols in Los Angeles and its implication for fine particulate matter composition and oxidative potential. Atmos. Environ. 133, 112–122.
Schwarz, J., Cusack, M., Karban, J., Chalupnickova, E., Havranek, V., Smolik, J., et al., 2016. PM2.5 chemical composition at a rural background site in Central Europe, including correlation and air mass back trajectory analysis. Atmos. Res. 176, 108–120.
Shahsavani, A., Naddafi, K., Jaafarzadeh Haghighifard, N., Mesdaghinia, A., Yunesian, M., Nabizadeh, R., et al., 2012. Characterization of ionic composition of TSP and PM10 during the middle eastern dust (MED) storms in Ahvaz, Iran. Environ. Monit. Assess. 184, 6683–6692.
Snyder, D.C., Rutter, A.P., Collins, R., Worley, C., Schauer, J.J., 2009. Insights into the origin of water soluble organic carbon in atmospheric fine particulate matter. Aerosol Sci. Technol. 43, 1099–1107.
Squizzato, S., Masiol, M., Agostini, C., Visin, F., Formenton, G., Harrison, R.M., et al., 2016. Factors, origin and sources affecting PM1 concentrations and composition at an urban background site. Atmos. Res. 180, 262–273.
Sun, Y.L., Chen, C., Zhang, Y.J., Xu, W.Q., Zhou, L.B., Cheng, X.L., et al., 2016. Rapid formation and evolution of an extreme haze episode in Northern China during winter 2015. Sci. Rep. 6.
Surratt, J.D., Lewandowski, M., Offenberg, J.H., Jaoui, M., Kleindienst, T.E., Edney, E.O., et al., 2007. Effect of acidity on secondary organic aerosol formation from isoprene. Environ. Sci. Technol. 41, 5363–5369.
Szidat, S., Jenk, T.M., Gaggeler, H.W., Synal, H.A., Fisseha, R., Baltensperger, U., et al., 2004. Radiocarbon (C-14)-deduced biogenic and anthropogenic contributions to organic carbon (OC) of urban aerosols from Zurich, Switzerland. Atmos. Environ. 38, 4035–4044.
Tan, J.-H., Duan, J.-C., Ma, Y.-L., Yang, F.-M., Cheng, Y., He, K.-B., et al., 2014. Source of atmospheric heavy metals in winter in Foshan, China. Sci. Total Environ. 493, 262–270.
Wahlin, P., Berkowicz, R., Palmgren, F., 2006. Characterisation of traffic-generated particulate matter in Copenhagen. Atmos. Environ. 40, 2151–2159.
Wang, X., Bi, X., Sheng, G., Fu, J., 2006. Hospital indoor PM10/PM2.5 and associated trace elements in Guangzhou, China. Sci. total Environ. 366, 124–135.
Wang, X., Chen, Y., Tian, C., Huang, G., Fang, Y., Zhang, F., et al., 2014a. Impact of agricultural waste burning in the Shandong Peninsula on carbonaceous aerosols in the Bohai Rim, China. Sci. total Environ. 481, 311–316.
Wang, Y.S., Yao, L., Wang, L.L., Liu, Z.R., Ji, D.S., Tang, G.Q., et al., 2014b. Mechanism for the formation of the January 2013 heavy haze pollution episode over central and eastern China. Sci. China Earth Sci. 57, 14–25.
Weber, R.J., Sullivan, A.P., Peltier, R.E., Russell, A., Yan, B., Zheng, M., et al., 2007. A study of secondary organic aerosol formation in the anthropogenic-influenced southeastern United States. J. Geophys. Res. Atmos. 112 (n/a-n/a).
Wu, R.R., Li, J., Hao, Y.F., Li, Y.Q., Zeng, L.M., Xie, S.D., 2016. Evolution process and sources of ambient volatile organic compounds during a severe haze event in Beijing, China. Sci. Total Environ. 560, 62–72.
Xin, J., Wang, L., Wang, Y., Li, Z., Wang, P., 2011. Trends in aerosol optical properties over the Bohai Rim in Northeast China from 2004 to 2010. Atmos. Environ. 45, 6317–6325.
Yearbook, C., 2014. China Statistical Yearbook.
Zhang, F., Chen, Y., Tian, C., Wang, X., Huang, G., Fang, Y., et al., 2014a. Identification and quantification of shipping emissions in Bohai Rim, China. Sci. Total Environ. 497, 570–577.
Zhang, R., Jing, J., Tao, J., Hsu, S.C., Wang, G., Cao, J., et al., 2013. Chemical characterization and source apportionment of PM2.5 in Beijing: seasonal perspective. Atmos. Chem. Phys. 13, 7053–7074.
Zhang, Y.L., Liu, J.W., Salazar, G.A., Li, J., Zotter, P., Zhang, G., et al., 2014b. Micro-scale (μg) radiocarbon analysis of water-soluble organic carbon in aerosol samples. Atmos. Environ. 97, 1–5.
Zhang, Y.L., Li, J., Zhang, G., Zotter, P., Huang, R.J., Tang, J.H., et al., 2014c. Radiocarbon-based source apportionment of carbonaceous aerosols at a regional background site on Hainan Island, South China. Environ. Sci. Technol. 48, 2651–2659.
Zong, Z., Chen, Y., Tian, C., Fang, Y., Wang, X., Huang, G., et al., 2015. Radiocarbon-based impact assessment of open biomass burning on regional carbonaceous aerosols in North China. Sci. Total Environ. 518–519, 1–7.